arXiv:2202.04442v1 [cond-mat.mes-hall] 9 Feb 2022

High Precision, Low Excitation Capactiance Measurement Methods from 10 mK- to Room-Temperature

Lili Zhao,[1] Wenlu Lin,[1] Xing Fan,[2] Yuanjun Song,[3] Hong Lu,[2] and Yang Liu[1]
[1)] *International Center for Quantum Materials, Peking University, Beijing, China, 100871*
[2)] *College of Engineering and Applied Sciences, Nanjing University, Nanjing, China, 210093*
[3)] *Beijing Academy of Quantum Information Sciences, Beijing, China, 100193*

(*Electronic mail: liuyang02@pku.edu.cn)

(Dated: 10 February 2022)

Capacitance measurement is a useful technique in studying quantum devices, as it directly probes the local particle charging properties, i.e. the system compressibility. Here we report one approach which can measure capacitance from mK to room temperature with excellent accuracy. Our experiments show that such a high-precision technique is able to reveal delicate and essential properties of high-mobility two-dimensional electron systems.

I. INTORDUCTION

Capacitance contains useful information of electronic devices, as it directly probes their electrical charging properties[1–7]. Recently, the capacitance measurement at cryogenic temperature has attracted significant attention in quantum studies and has revealed a series of quantum phenomena[8–16]. Although high precision capacitance measurement is widely used in studying classical devices such as field effect transistors and diodes, it is extremely difficult to be performed on quantum devices. Firstly, the quantum phenomena usually emerge in fragile systems so that the excitation should be sufficiently low to preserve the quantum properties of the device. Secondly, many quantum devices can only be studied in cryostats which host the low temperature and high magnetic field environment. The meter-long cables connecting samples and room temperature instruments have $\sim$ 100 pF capacitance, which is orders-of-magnitude larger than the devices themselves. Thirdly, the total power dissipation at the cryogenic sample stage must be limited to sub-μW in order to maintain the low-temperature environment. This limits the use of active devices.

In order to reduce the crosstalk and signal leaking between cables, many reported works use the cryogenic preamplifier to isolate the input and output signals[5,10,11,17,18]. Unfortunately, the preamplifiers usually dissipate more than $\sim$10 μW heat at the sample stage, which is sufficiently high to cause a noticeable temperature raise. Sometimes, indirect probs of capacitance such as penetration field, etc, are used which can provide qualitative information about quantum phase transitions[7,12–15].

In this report, we introduce a new approach for high precision capacitance measurement from 10 mK- to room-temperature. We install a passive bridge at the sample stage, and use a voltage-controlled-variable-resistance to in-situ tune its balance. We use radio frequency excitation to increase the output signal, and develop a high sensitivity redio frequency (RF) lock-in technique to analyze the bridge output.

II. METHOD

The passive bridge at the sample stage (Fig. 1(a)) consists of the device under test $C_{\rm DUT}$, the reference capacitor $C_{\rm ref}$, the reference resistor $R_{\rm ref}$ and a voltage-controlled-variable-resistor $R_{\rm h}$. The excitation voltage $V_{\rm in}$ is differentially coupled to the $V_{\rm in}^{+}$ & $V_{\rm in}^{-}$ ports of the bridge by a RF transformer, and the output signal $V_{\rm out}$ is the voltage difference between the midpoints of the capacitor and resistor arms. The bridge dissipates only $\sim$ 10 nW when $V_{\rm in} \simeq 1$ mV$_{\rm rms}$, mostly caused by $R_{\rm ref}$ and $R_{\rm h}$. We can tune the balance of the bridge with $R_{\rm h}$, which is the drain-to-source resistance of a high electron mobility transistor (model ATF35143). The bridge reaches it's balance point when the balance condition

$$\frac{C_{\rm DUT}}{C_{\rm ref}} = \frac{R_{\rm h}}{R_{\rm ref}}. \tag{1}$$

is achieved, signaled by the $|V_{\rm out}|$ minimum (see Fig. 1(b)). Two low-frequency current inputs I_1 and I_2 are injected into the bridge. They flow into the ground through $R_{\rm h}$ and $R_{\rm ref}$, respectively, and generate a voltage difference $(V_{\rm R}^{+} - V_{\rm R}^{-}) = I_1 \cdot R_{\rm h} - I_2 \cdot R_{\rm ref}$. We can in-situ measure $R_{\rm h}$ and $R_{\rm ref}$ simultaneously with lock-in technique by locking the frequency of $(V_{\rm R}^{+} - V_{\rm R}^{-})$ to be the same as I_1 and I_2. Therefore, as long as $C_{\rm ref}$ is stable, the absolute value of $C_{\rm DUT}$ can be deduced by Eq.1. The $|V_{\rm out}|$ vs. $R_{\rm h}$ curve is "V"-shaped, so we call this procedure as the "V-curve" procedure for brevity.

The output impedance of this bridge is about $\frac{1}{2\pi f(C_{\rm ref}+C_{\rm DUT})}$, where f is the frequency of $V_{\rm in}$. $C_{\rm DUT}$ and $C_{\rm ref}$ are typically in the order of 0.1 pF, corresponding to output impedance as large as $\sim$ 1 GΩ when $f = 1$ kHz. Therefore, we increase f to $\sim$ 100 MHz so that the output impedance decreases to about 10 kΩ. we use standard 50 Ω coaxial cable and impedance matched RF preamplifier at room temperature for broadband measurement. When the excitation amplitude is $\simeq$ 1mV$_{\rm rms}$, $V_{\rm out}$ is only about ~ 1 μV$_{\rm rms}$ and 0.1% change in $C_{\rm DUT}$ corresponds to $\simeq$ 1 nV$_{\rm rms}$ variation in the output. In order to analyze such a small signal, we combine the superheterodyne and lock-in techniques (see Fig. 1(c)). The signal source generates three single-frequency signals $V_{\rm in}$, $V_{\rm LO}$ and $V_{\rm ref}$ with frequencies $f_{\rm in}$, $f_{\rm LO}$ and $f_{\rm d}$, respectively, where $f_{\rm d} = |f_{\rm in} - f_{\rm LO}|$. $V_{\rm in}$ is sent to the bridge as the voltage excitation. The bridge output $V_{\rm out}$ is amplified by a low-noise-amplifier, mixed with $V_{\rm LO}$

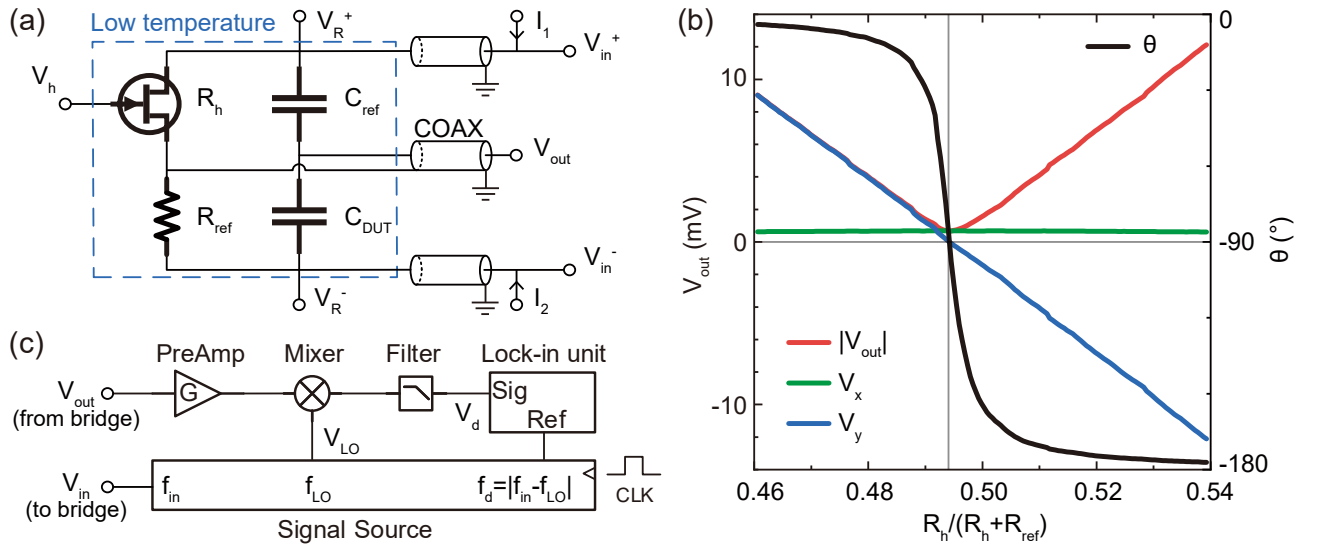


FIG. 1. Schematic diagram of our measurement setup. (a) The passive capacitance bridge installed at the sample stage consists $C_{\rm DUT}$, $C_{\rm ref}$, $R_{\rm ref}$ and $R_{\rm h}$. $R_{\rm h}$ can be tuned by $V_{\rm h}$. $V_{\rm in}^{+}$ and $V_{\rm in}^{-}$ are the two differentially coupled input signal, $V_{\rm out}$ is the output signal. Coaxial cables are used to improve the transmission efficiency and minimize the parasitic capacitance. I_1 and I_2 are two quasi-DC current inputs with different frequencies, $R_{\rm h}$ ($R_{\rm ref}$) can be deduced by analyzing the frequency component same as I_1 (I_2) of the differential voltages between $V_{\rm R}^{+}$ and $V_{\rm R}^{-}$. (b) One typical result of the "V-curve" procedure. The cross point is the balance point of the bridge, signaled by the $|V_{\rm out}|$ minimum, and $C_{\rm DUT}$ can be calculated using Eq. (1). $V_{\rm out}$ can be decomposed into $V_{\rm y}$ and $V_{\rm x}$. $V_{\rm x}=0$ at the balancing point and depends on $\frac{R_{\rm h}}{R_{\rm ref}+R_{\rm h}}$ linearly. (c) Diagram of the radio-frequency lock-in setup. The bridge output $V_{\rm out}$ passes through a room-temperature amplifier (PreAmp), a mixer (Mixer) and a low pass filter (Filter) and turns into a low frequency signal $V_{\rm d}$ whose frequency is $f_{\rm d}=|f_{\rm in}-f_{\rm LO}|$. $V_{\rm d}$ is then analyzed by an audio-frequency digital lock-in unit.

and low-pass-filtered, resulting in an audio frequency signal $V_{\rm d}$. We use a digital audio-frequency lock-in unit to measure the amplitude $|V_{\rm d}|$ and phase $\theta_{\rm d}$ in reference to $V_{\rm ref}$, where $|V_{\rm d}|\propto|V_{\rm out}|$ and $\theta_{\rm d}$ is the same as the phase difference between $V_{\rm out}$ and $V_{\rm in}$ but differs by a constant. For simplicity, we quote $|V_{\rm d}|$ and $\theta_{\rm d}$ as the amplitude $|V_{\rm out}|$ and the (relative) phase θ (from $V_{\rm in}$) of the bridge output.

III. CALIBRATION

We calibrate our setup at room temperature by measuring fixed-value capacitors whose nominal value $C_{\rm nom}$ ranges from 0.1 to 10 pF (see Fig. 2(a)). We select different $C_{\rm ref}$ that is comparable with $C_{\rm DUT}$. The y-axis is the measured $C_{\rm DUT}$ using the "V-curve" procedure with $\simeq 1.5\ {\rm mV_{rms}}$ excitation amplitude and $\simeq 110$ MHz frequency. The horizontal and vertical error bars are deduced from the tolerance of $C_{\rm DUT}$ and $C_{\rm ref}$, which dominate the inaccuracy at <1 pF. The measured $C_{\rm DUT}$ matchs its nominal value $C_{\rm nom}$ even for capacitors as small as 0.1 pF, evidencing that our setup is capable of measuring the absolute capacitance value[19].

The "V-curve" procedure can measure the absolute value of $C_{\rm DUT}$ with decent accuracy, however, continuously monitoring $C_{\rm DUT}$ while sweeping particular physical parameter, such as magnetic field, temperature, etc, is of more interest. We can deduce $C_{\rm DUT}$ from $V_{\rm out}$ using the $V_{\rm out}$ vs. $R_{\rm h}$ relation obtained by the "V-curve" procedure. At the vicinity of the balance point, the bridge output $V_{\rm out}$ is approximated as

$$V_{\rm out}\propto\left(\frac{C_{\rm DUT}}{C_{\rm ref}+C_{\rm DUT}}-\frac{R_{\rm h}}{R_{\rm ref}+R_{\rm h}}\right)\cdot V_{\rm in}+V_0, \tag{2}$$

where V_0 represents the leaking signal. $V_{\rm out}$ is a vector and can be decomposed into two orthogonal scalar components using its amplitude $|V_{\rm out}|$ and phase θ

$$\begin{cases} V_{\rm x}=|V_{\rm out}|\cdot\cos(\theta), \\ V_{\rm y}=|V_{\rm out}|\cdot\sin(\theta), \end{cases} \tag{3}$$

Note that, in the ideal case when $V_0=0$, $V_{\rm out}$ changes its sign, or θ changes by 180° as we tune the bridge through its balance point. We set $\theta=-90^\circ$ at the balance point so that $V_{\rm x}=V_{\rm out}$ is the expected bridge output (Fig. 1(b)). In a careful measurement, leaking signal V_0 mostly comes from the capacitive coupling between the input and output cables and has a 90° phase shift from $V_{\rm in}$. At the vicinity of the balance point, $V_{\rm y}\approx V_0$ and $V_{\rm x}$ has a linear dependence on $\frac{R_{\rm h}}{R_{\rm ref}+R_{\rm h}}$, see Fig. 1(b). From the symmetry between the resistors and capacitors in the bridge, we assume a single parameter, the sensitivity S, can describe the dependence of $V_{\rm x}$ on both $R_{\rm h}$ and $C_{\rm DUT}$ by

$$S=\frac{\partial V_{\rm x}}{\partial\frac{R_{\rm h}}{R_{\rm ref}+R_{\rm h}}}=\frac{\partial V_{\rm x}}{\partial\frac{C_{\rm DUT}}{C_{\rm ref}+C_{\rm DUT}}}. \tag{4}$$

S can be obtained by linearly fitting $V_{\rm x}$ with $\frac{R_{\rm h}}{R_{\rm ref}+R_{\rm h}}$ while keep $C_{\rm DUT}$ fixed. Note that S is inversely proportional to the output impedance $1/2\pi f(C_{\rm ref}+C_{\rm DUT})$ and corresponding corrections might be necessary. Thereafter, we can deduce $C_{\rm DUT}$

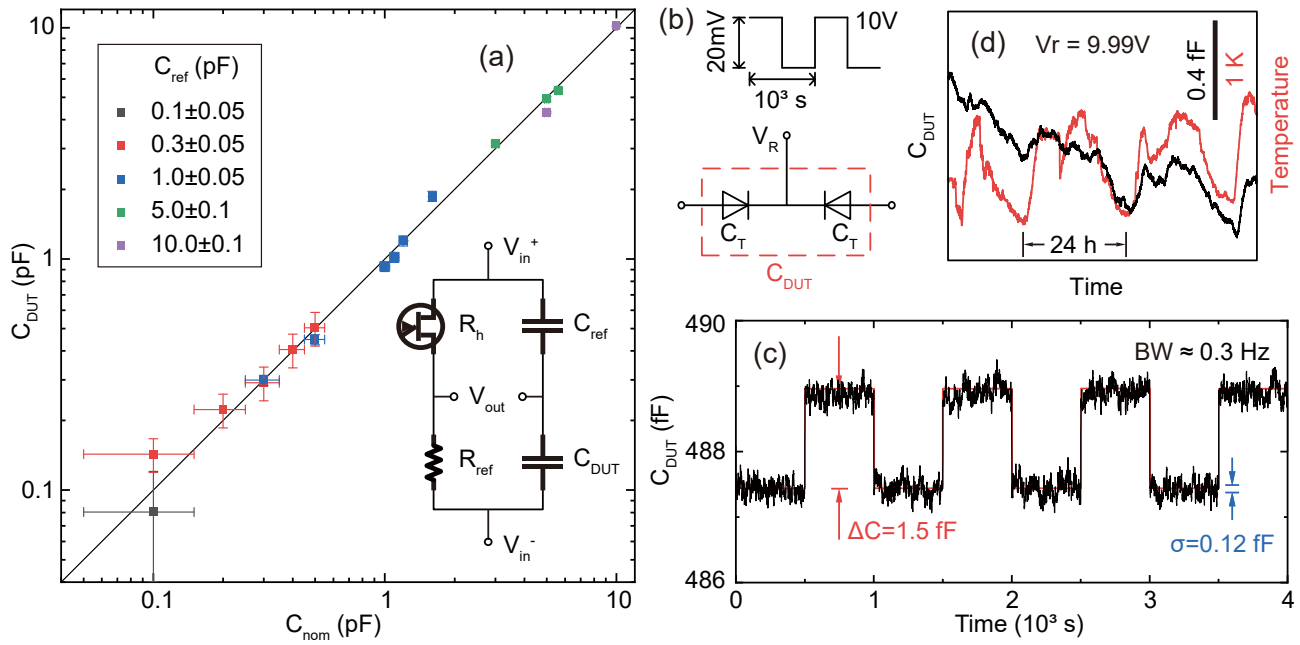


FIG. 2. Room temperature examination of our setup. (a) $C_{\rm DUT}$ is the measured capacitors values using the "V-curve" procedure. $C_{\rm nom}$ is their nominal value given by manufacturers, and the error bar is deduced from their tolerance. The black line is the ideal $C_{\rm DUT} = C_{\rm nom}$. Different colors of point data represent different $C_{\rm ref}$ used. (b) Measuring two tunable capacitance diodes in series. The reverse voltage $V_{\rm R}$ tunes the value of each diode capacitance $C_{\rm T}$. $V_{\rm R}$ is a 1000-second-period, square wave with high/low voltages equal 10/9.98 V. (c) Measured $C_{\rm DUT}$. $C_{\rm DUT} \approx 487.5$ fF for $V_{\rm R} = 10V$, and increases by 1.5 fF when $V_{\rm R}$ decreases by 20 mV. The standard deviation is as low as 0.1 fF at 0.3 Hz measurement bandwidth. (d) Long period monitoring of $C_{\rm DUT}$ with $V_{\rm R}$ fixed at 9.99 V (black), as well as the room temperature (red).

from $V_{\rm out}$ by

$$\frac{C_{\rm DUT}}{C_{\rm ref}+C_{\rm DUT}} = \frac{R_{\rm h}}{R_{\rm ref}+R_{\rm h}} - \frac{V_{\rm x}}{S}. \qquad (5)$$

Figs. 2(b-d) examine the feasibleness of the "monitoring"-mode. The device-under-test is two back-to-back connected tunable capacitance diodes (Infineon BB837) whose capacitance $C_{\rm T}$ can be controlled by the diode reverse voltage $V_{\rm R}$. $V_{\rm R}$ has a 9.99 V DC component which biases $C_{\rm DUT} = 0.5C_{\rm T}$ to about 500 fF, as well as a 20 $\rm mV_{pp}$, 1000-second-period square-wave AC component which induces a small capacitance variation, see Fig. 2(b). The frequency and amplitude of $V_{\rm in}$ are 110 MHz and $\sim$1 $\rm mV_{rms}$, respectively. We show the measured capacitance using the "monitoring"-mode in Fig. 2(c). The measured $C_{\rm DUT}$ is about 487.5 fF when $V_{\rm R}$=10 V, and increases by 1.5 fF when $V_{\rm R}$ decreases by 20mV; consistent with the BB837 datasheet. The standard deviation of $C_{\rm DUT}$ is about 0.12 fF at 0.3 Hz measurement bandwidth[20]. In short, this method can resolve $\lesssim$ 240 ppm variation of a $\simeq$ 0.5 pF capacitor within a few second. Fig. 2(d) shows $C_{\rm DUT}$ measured for 72 hours, which drifts by $<$ 1 fF in 72 h. The variation of $C_{\rm DUT}$ is in good agreement with the room temperature fluctuation, likely introduced by the device itself.

IV. MEASUREMENTS AT MK-TEMPERATURE

We install the capacitance setup into an Oxford Triton 400 dilution refrigerator, and study the gate-to-2D capacitance of a high-mobility two-dimensional electron gas (2DEG) sample at mK temperature in Fig. 3[21]. The sample consists an AlGaAs/GaAs/AlGaAs quantum well structure grown by molecular beam epitaxy, as illustrated in Fig. 3(a). The mobility is about 2 $\rm m^2/(V\cdot s)$. The 650-Å-wide GaAs quantum well resides 1665 Å below the surface, bound by AlGaAs spacer-layers on both sides. We grow three Si-δ-doping-layers in the spacer-layers, two in the surface-side one, and one in the substrate-side one. At zero front gate bias, a bilayer-like 2DEG forms inside the quantum well, and another 2DEG forms at the interface between the substrate-side AlGaAs spacer-layer and the GaAs buffer-layer, see Fig. 3(a). We evaporate two concentric gates and measure the gate-to-gate capacitance, i.e. the two gate-to-2D capacitors which are serial-connected by the 2DEG. The inner gate radius is 60 μm, and the gap between the two gates is 20 μm. The outer-gate is much bigger than the inner-gate, so that $C_{\rm DUT}$ is approximately the inner-gate-to-2D capacitance. An isolation capacitor[22] is used between the inner-gate and the bridge so that a DC gate bias $V_{\rm FG}$ can be applied. The frequency and amplitude of $V_{\rm in}$ is 17 MHz and $\sim$0.4 $\rm mV_{rms}$, respectively. We don't see any increase of the mixing chamber temperature ($\lesssim$ 17 mK) when turn on the measurement, evidencing that the heat load at the sample stage is negligible[21].

Fig. 3(b) shows the $C_{\rm DUT}$ as a function of $V_{\rm FG}$ measured at 250 mK[23]. The electron charging falls into four scenarios, corresponding to the four plateaus seen in the Fig. 3(b) data. Depletion: The 2DEG under the inner-gate is completely de-

TABLE I. The parameters of 2DEG learnt by our measurement. The subscript $i = 1,2,3$ indicates the parameter in cases I, II and III, respectively.

Cases	$C^i_{\rm DUT}$ (pF)	d_i (Å)	ΔV_i (V)	n_i ($10^{11} cm^{-2}$)	V^i_B (V)
I	1.95	3500	2.03	4.17	0.33
II	3.01	2273	0.52	1.64	0.20
III	3.57	1913	0.68	2.55	0.19
I:II:III	1:1.54:1.83	1/(1:1.54:1.83)	\	1:0.39:0.61	1/(1:1.65:1.74)

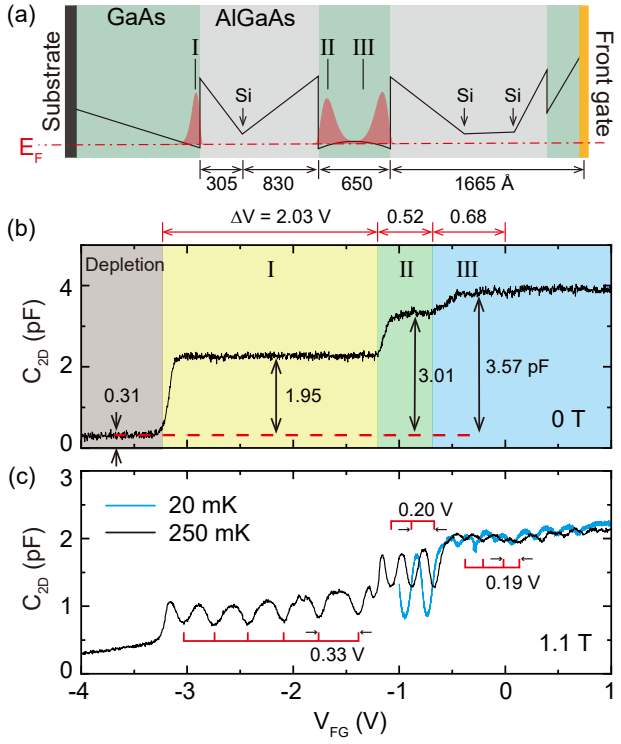


FIG. 3. Studying high-mobility 2DEG in GaAs/AlGaAs heterostructure samples with capacitance measurement. (a) Sample structure. Black, green, gray and yellow regions represents the substrate, the GaAs layer, the AlGaAs layer and the metallic front gate, respectively. The black solid line represents the conduction band edge and the red dash-dot line is the Fermi level $E_{\rm F}$. The vertical arrow indicates the δ-doping positions. The red shaded areas represent the charge distribution of 2DEG at zero gate voltage. I, II and III indicate the effective charge position of the top-most 2DEG in the three cases of (b). (b) The measured gate-to-2D capacitance $C_{\rm 2D}$. The four $C_{\rm 2D}$ plateaus indicate four different working senario of the device: Depletion, Cases I, II and III. The black and red double-arrow lines marks the capacitance value and the voltage range for each plateau. (c) $C_{\rm 2D}$ vs. $V_{\rm FG}$ at 1.1 T perpendicular magnetic field. The red lines mark the periods of oscillation of the 250-mK trace.

pleted when $V_{\rm FG}$ is small and the $C_{\rm DUT}$ is close to zero. Case I: As $V_{\rm FG}$ increases, the first 2DEG starts to form at the interface between the buffer-layer and substrate-side spacer-layer. Case II: The second 2DEG forms at the substrate-side interface of the quantum well when $V_{\rm FG}$ reaches -1.20 V. Case III: Keep increasing $V_{\rm FG}$ increases the charge density inside the quantum well as well as makes it more symmetric. The effective charging position becomes close to the quantum well center when electrons starts to fill the second subband, whose charge distribution locates at the surface-side interface of the quantum well.

The $C_{\rm DUT} = 0.31$ pF in the depletion region is likely the stray capacitance of the inner gate. We subtract it from the measured capacitances and summarize the plateau heights corresponding to cases I, II, and III in Table I as $C^i_{\rm DUT}$, $i = 1,2,3$ (see also Fig. 3(b)). Note that $C^i_{\rm DUT}$ is inversely proportional to d_i, the distance between the surface and the effective position of the topmost 2DEG[6]. $d_1 \approx 3500$Å because the effective position of a heterojunction 2DEG is estimated to be $\simeq$50 Å away from the interface[24]. We then calculate d_2 and d_3 using the relation $C^i_{\rm DUT}/C^j_{\rm DUT} = d_j/d_i$ and list them in Table I. These results suggest that the effective position of the quantum-well 2DEG is about 42 Å ($= 2315$Å $- d_2$) away from its substrate-side interface when it first appears, and moves to 248 Å ($= d_1 - 1665$Å) away from its surface-side interface when electron occupies the second-subband. A comprehensive investigation may track this evolution more thoroughly, which is out of our scope here.

When subjected into a large perpendicular magnetic field B, the electrons of a 2DEG are quenched into discrete Landau levels, leading to density-dependent compressibility. When we tune the 2DEG density by sweeping $V_{\rm FG}$ (see Fig. 3(c)), we observe a $C_{\rm DUT}$ oscillation where each period corresponds to the occupation of two Landau levels (two spins) in the topmost 2DEG[16]. we extracted the oscillation period V^i_B for the three cases and list them in Table I. The reciprocal ratio of V^i_B is similar to the ratio of $C^i_{\rm DUT}$, consistent with our expectation that $C^i_{\rm DUT}$ is inversely proportional to V^i_B as $C^i_{\rm DUT} \propto \frac{2Be^2}{h}/V^i_B$, where h is the Planck's constant, e is the electron charge and B is the magnetic field. Note that the capacitance oscillation is strong in Case I and II, but heavily damped in Case III. At lower temperature 20 mK, the oscillation becomes more pronounced in case II, but remain roughly unchanged in case III. This is possibly because the two subbands have spatially separated charge distribution which smooths the compressibility oscillation.

We can also calculate the density of each 2DEG using the relation $n_i = \frac{\varepsilon_{\rm r}\varepsilon_0}{e} \cdot \Delta V_i/d_i$, where $\varepsilon_{\rm r} = 13$ is the relative dielectric constant, ε_0 is the permittivity of vacuum and ΔV_i is the width of the plateau in the Case-i region, see Fig. 3(b). We find that $n_2/n_1 = 0.39$ agrees with the reciprocal ratio of the distance from the doping layer to the corresponding 2DEG (355 Å : 872Å $= 0.41$, see Fig. 3(a)).

V. CONCLUSION

We have introduced a high-precision, low-excitation capacitance measurement method for 10 mK- to room-temperature experiments. We are able to measure the absolute capacitance value using the "V-curve" procedure, and monitor the variation of capacitor using $V_{\rm out}$. With about 1 $\rm mV_{rms}$ excitation voltage, we can resolve 240 ppm variation of a 500 fF capacitor. We measure the gate-to-2D capacitance of a high-mobility two-dimensional electron system at mK-temperature and extract consistent, essential information of the device. The results demonstrate that our capacitance bridge can detect extremely small capacitance fluctuation with mV-excitation at 10 mK-temperature.

ACKNOWLEDGMENTS

Y. Liu acknowledge support by the National Basic Research Program of China (Grant No. 2019YFA0308403) and the National Natural Science Foundation of China (Grant No. 92065104 and 12074010) for sample fabrication and measurement. H. Lu acknowledges the support from the National Key R&D Program of China (2018YFA0306200) and the National Natural Science Foundation of China (Grant No. 51732006) for material growth. We thank M. Shayegan, Lloyd Engle, Jianhao Chen and Xi Lin for valuable discussion.

[1] M. Kaplit and J. N. Zemel, "Capacitance observations of landau levels in surface quantization," Phys. Rev. Lett. **21**, 212–215 (1968).

[2] A. M. Voshchenkov and J. N. Zemel, "Admittance studies of surface quantization in [100]-oriented si metal-oxide-semiconductor field-effect transistors," Phys. Rev. B **9**, 4410–4421 (1974).

[3] T. P. Smith, B. B. Goldberg, P. J. Stiles, and M. Heiblum, "Direct measurement of the density of states of a two-dimensional electron gas," Phys. Rev. B **32**, 2696–2699 (1985).

[4] V. Mosser, D. Weiss, K. Klitzing, K. Ploog, and G. Weimann, "Density of states of gaas-algaas-heterostructures deduced from temperature dependent magnetocapacitance measurements," Solid State Communications **58**, 5–7 (1986).

[5] R. C. Ashoori, H. L. Stormer, J. S. Weiner, L. N. Pfeiffer, S. J. Pearton, K. W. Baldwin, and K. W. West, "Single-electron capacitance spectroscopy of discrete quantum levels," Phys. Rev. Lett. **68**, 3088–3091 (1992).

[6] J. Jo, E. A. Garcia, K. M. Abkemeier, M. B. Santos, and M. Shayegan, "Probing the subband structure of a wide electron system in a parabolic quantum well via capacitance-voltage measurements," Phys. Rev. B **47**, 4056–4059 (1993).

[7] J. P. Eisenstein, L. N. Pfeiffer, and K. W. West, "Compressibility of the two-dimensional electron gas: Measurements of the zero-field exchange energy and fractional quantum hall gap," Phys. Rev. B **50**, 1760–1778 (1994).

[8] T. P. Smith, W. I. Wang, and P. J. Stiles, "Two-dimensional density of states in the extreme quantum limit," Phys. Rev. B **34**, 2995–2998 (1986).

[9] M. J. Yang, C. H. Yang, B. R. Bennett, and B. V. Shanabrook, "Evidence of a hybridization gap in "semimetallic" inas/gasb systems," Phys. Rev. Lett. **78**, 4613–4616 (1997).

[10] B. M. Hunt, J. I. A. Li, A. A. Zibrov, L. Wang, T. Taniguchi, K. Watanabe, J. Hone, C. R. Dean, M. Zaletel, R. C. Ashoori, and A. F. Young, "Direct measurement of discrete valley and orbital quantum numbers in bilayer graphene," Nature Communications **8**, 948 (2017).

[11] S. L. Tomarken, Y. Cao, A. Demir, K. Watanabe, T. Taniguchi, P. Jarillo-Herrero, and R. C. Ashoori, "Electronic compressibility of magic-angle graphene superlattices," Phys. Rev. Lett. **123**, 046601 (2019).

[12] J. P. Eisenstein, L. N. Pfeiffer, and K. W. West, "Negative compressibility of interacting two-dimensional electron and quasiparticle gases," Phys. Rev. Lett. **68**, 674–677 (1992).

[13] A. A. Zibrov, C. Kometter, H. Zhou, E. M. Spanton, T. Taniguchi, K. Watanabe, M. P. Zaletel, and A. F. Young, "Tunable interacting composite fermion phases in a half-filled bilayer-graphene landau level," Nature **549**, 360–364 (2017).

[14] A. A. Zibrov, P. Rao, C. Kometter, E. M. Spanton, J. I. A. Li, C. R. Dean, T. Taniguchi, K. Watanabe, M. Serbyn, and A. F. Young, "Emergent dirac gullies and gully-symmetry-breaking quantum hall states in *aba* trilayer graphene," Phys. Rev. Lett. **121**, 167601 (2018).

[15] H. Deng, L. N. Pfeiffer, K. W. West, K. W. Baldwin, L. W. Engel, and M. Shayegan, "Probing the melting of a two-dimensional quantum wigner crystal via its screening efficiency," Phys. Rev. Lett. **122**, 116601 (2019).

[16] H. Irie, T. Akiho, and K. Muraki, "Determination of g-factor in InAs two-dimensional electron system by capacitance spectroscopy," Applied Physics Express **12**, 063004 (2019).

[17] A. Hazeghi, J. A. Sulpizio, G. Diankov, D. Goldhaber-Gordon, and H. S. P. Wong, "An integrated capacitance bridge for high-resolution, wide temperature range quantum capacitance measurements," Rev. Sci. Instrum. **82**, 053904 (2011).

[18] G. J. Verbiest, H. Janssen, D. Xu, X. Ge, M. Goldsche, J. Sonntag, T. Khodkov, L. Banszerus, N. von den Driesch, D. Buca, K. Watanabe, T. Taniguchi, and C. Stampfer, "Integrated impedance bridge for absolute capacitance measurements at cryogenic temperatures and finite magnetic fields," Rev. Sci. Instrum. **90**, 084706 (2019).

[19] In Fig. 2(a), $C_{\rm DUT}$ slightly deviates from $C_{\rm nom}$ when $C_{\rm DUT} \neq C_{\rm ref}$. This is not surprising because the bridge output is less sensitive to $C_{\rm DUT}$ in theis case, so that the leaking signal causes more deviation.

[20] The equivalent voltage noise of the whole setup at the input of the RF preamplifier has a spectrum density of about 8 $\rm nV/\sqrt{Hz}$.

[21] The mixing chamber temperature increases from $\simeq$ 8 mK to $\simeq$ 17 mK after we install three semi-rigid coaxial cables. In a separate report, we use extra-thin flexible coaxial wires and the mixing chamber temperature can be kept below 10 mK during the measurement[25].

[22] The isolation capacitor is 22 nF in this measurement, which needs to be much larger than the device capacitance.

[23] In this manuscript, all quoted temperatures are mixture chember plate temperatures of the dilution refrigerator.

[24] T. Ando, A. B. Fowler, and F. Stern, "Electronic properties of two-dimensional systems," Rev. Mod. Phys. **54**, 437–672 (1982).

[25] L. Zhao, W. Lin, Y. J. Chung, K. W. Baldwin, L. N. Pfeiffer, and Y. Liu, "Capacitive response of wigner crystals at the quantum hall plateau," (2022), arXiv:2201.06203.